applied sciences

MDPI

Article

Colour Ageing in Acrylic Resin Plates and Natural Minerals on the Façade after 10 Years of Sun Exposure in the Marine Environment

Ángel Benigno González-Avilés *, Víctor Echarri-Iribarren, Antonio Galiano-Garrigós, Carlos Rizo-Maestre and María Isabel Pérez-Millán

Department of Architectural Constructions, University of Alicante, 03690 Alicante, Spain; victor.echarri@ua.es (V.E.-I.); antonio.galiano@ua.es (A.G.-G.); carlosrm@ua.es (C.R.-M.); isabel.perez@ua.es (M.I.P.-M.)

* Correspondence: angelb@ua.es

Abstract: The synthetic material developed by Dupont in 1963 for solid surfaces has been used since its origin for numerous applications. One of the most popular ones in the last decade is as a finishing layer on façades. The first references that contemplated this use on the outside were the Seeko'o hotel in Bordeaux executed in 2007 and the refurbishment of the 7700 m^2 shell of the Hôtel Ivoire congress centre in Abidjan (Ivory Coast) in 2009. In Spain, the first example of the installation of this material is the rehabilitation of the main building of the La Rotonda de la Playa de San Juan urbanisation in Alicante, designed in 1965 by the architect Juan Guardiola Gaya and rehabilitated in 2010 by Miguel Salvador Landmann. Ten years later, our research is focused on the study of the colour ageing of the acrylic resin and natural mineral sheets on each of its façades, with different orientations and exposure to sea and wind. To this end, it has been studied the solar radiation of the surfaces, the wind exposure of their façades and tests with a tele-spectroradiometer has been carried out. The study makes it possible to quantify the differences in colour in all of them and to state that the combination of wind and radiation is the main atmospheric agent causing the degradation.

Keywords: constitutive modelling; colour; rehabilitation; marine exposure; constructive ageing; colourimetry; BIM

Citation: González-Avilés, Á.B.; Echarri-Iribarren, V.; Galiano-Garrigós, A.; Rizo-Maestre, C.; Pérez-Millxaxn, M.I. Colour Ageing in Acrylic Resin Plates and Natural Minerals on the Façade after 10 Years of Sun Exposure in the Marine Environment. *Appl. Sci.* **2021**, *11*, 2222. https://doi.org/10.3390/app11052222

Academic Editor: Tomasz M. Majka

Received: 5 January 2021
Accepted: 7 February 2021
Published: 3 March 2021

1. Introduction

During this century there have been large rehabilitation projects using new materials in façades with a great concern in ensuring that the useful life cycle of the material is high [1]. This characteristic is key when choosing a material [2]. The assumptions concerning the replacement, repair and maintenance of the material had to be as realistic as possible [3]. Over the last decade, much research has been carried out on new façade solutions and new materials to improve the energy efficiency of the building [4]. Energy production systems using photovoltaic materials [5], microalgae façades such as solar thermal collectors [6] and phase change materials [7] (PCM) [8] are being incorporated into envelopes to improve environmental comfort and reduce consumption [9]. In all of them, the quantification of solar radiation on the façade using virtual models is essential [10]. Thanks to Building Information Modelling (BIM) tools, it is possible to predict the behaviour of the envelope, calculate the radiation, transmittances and shadows of our buildings.

During this same time, many projects have arisen with the use of acrylic resin materials and natural minerals as a finishing coat on exterior façades. Their use in exteriors for more than ten years, allows to corroborate the tests of ageing in laboratory of the analytical method, testing empirically by means of field works. These tests, depending on the material, are costly, time-consuming and often unreliable [11].

It is known that the degradation of a façade is mainly caused behave perfectly when in contact with solar radiation and exposed to wind [12], hygrothermal ageing [13] by humidity [14] or rain [15], biological agents and pollution. Solar radiation in a country

like Spain and in a southern coastal area like Alicante is a fundamental aspect. Not so much because of the implementation of materials with the aim of improving efficiency, but because of the search for sustainability through the useful life of the material. For this reason, the material to be used in the rehabilitation of this building had to behave perfectly to solar radiation and exposure to wind in a marine environment over time.

There are many types of coatings that perform well in all three of these areas. A new coating or a new dry material could be used for rehabilitation. It was decided to use a shaped material that came from the workshop and lightened the weight. It could then be a plastic or metallic material. Monolithic panels and Metal/polymer/metal sandwich made of 100% recyclable aluminium composite were studied without losing quality and with high durability [16]. Various investigations [17] supported their placement. The project management did not want to place a metallic material as it was not feasible to generate the entire parapet in one piece. The metallic material was also discarded due to the predominant direction and intensity of the wind and the wetting and drying cycles with the presence of chlorides in a marine environment that could affect it. Finally, a synthetic material developed by Dupont was chosen.

2. Research Bibliography

Corian is characterized by its strength and thermoformability. Dupont manufactures this material composed by weight of 1/3 [18] of of polymethyl methacrylate acrylic resin (PMMA) and 2/3 of alumina trihydrate Al2O3.3H2O (ATH). Its characterization and emissions have been studied by Chaolong et al [19,20]. The density of Corian is about 1710 kg/m^3 [21]. Jackson et al. [22] determined the particle size 20 μm and the Young's modulus 10,000 MPa.

Made up of 1/3 acrylic resin (PMMA) and 2/3 aluminium hydroxide (aluminium trihydrate), the material Corian is characterised by its strength and thermoformability. Its use is linked to many areas, mainly in interiors, bathrooms, kitchens and hospital equipment, but also in general furniture pieces and in the last decade in façades. In this last application, compared to other façade materials, its high price is its only disadvantage. Its translucent capacity, ease of modelling and the possibility of making designs without apparent joints have made it an experimental material in many design works of this century.

Andriievska and Marchuk [23] made an extensive comparison of the characteristics of this material from five different manufacturers. They subject samples of TM Tristone (South Korea) Bitto Dongguan (China), Corian® (USA), Polystone (China) and LG Ni-macs (South Korea) to standard methods for the following parameters: density, water absorption, compressive strength, flexural strength, impact resistance, wear resistance, Mohs hardness and chemical resistance. However, they do not analyse colour degradation.

Research carried out by other authors shows the changes in the bending of the panels as a function of temperature [13] and their ductile behaviour at temperatures above 75 °C [24] or their ability to reach temperatures close to 82. 6 °C [25]. All of them show the reduction in the characteristics of the material at high temperatures, but not at temperatures below 0°.

Dupont branded material has a large number of certifications for outdoor application. Research by Basaran and Nie [26], funded by DuPont, into thermodynamic damage to the material already anticipated its superb properties [27].

Although some research has been carried out on ventilated façades executed with the material, the absence of a bibliography on such an important subject in architecture as colour is surprising. Dupont's classification for colour degradation ranges from less than or equal to 5ΔE*ab units, from 5 to 15 and above 15 to ten years [28]. In the case of exteriors even less than 2 for the models Glacier Ice and Designer White according to tests ASTM D2244 [29].

5ΔE^*_{ab} represents the difference in colour perceptible by the human eye between two points. It is difficult for the human eye to recognise values of ΔE* below 2 as a colour difference. Dozic´et al. have established that in order for a colour difference between two

teeth to be visually perceived under standardised conditions, ΔE* must take a value of 1, and a value above 3 under clinical conditions [30], so in the absence of contrast with another piece it is difficult to check this difference in a building.

As a result of its magnificent behaviour and despite its high price, at the end of the first decade of the 21st century its use in façades became widespread and almost ten years later it is possible to analyse the results. Other authors have begun to investigate composites that reduce the price of the material as a function of the percentage of filler in the composite [31] and how the increase in ATH concentration affects price reduction [32]. However, this manipulation implies the decrease of the bending resistance and the increase of hardness and bending modulus together with the density [33]. This aspect does not matter in interior uses but can cause problems in exterior and façades.

The new generation of materials perform well in terms of their mechanical properties. So far, preliminary colour assessment were made based on acellerated Weather-Ometer testing performed in accordance with ASTM G155.

This research provides the study of the colour degradation of the material empirically after 10 years of exposure.

3. Research Method and Material

The methodology consists of double research. The environmental conditions of exposure of the material and the colour degradation with respect to the original piece are evaluated. As a starting point, the measurement of solar radiation and the predominance of winds on the building is established.

Only a part of the broad spectrum of electromagnetic radiation from the sun reaches the earth's surface [34].

Most of the radiation that reaches from the sun is part of infrared radiation (IR), about 5% is Ultraviolet A (UVA) and 0.5% is Ultraviolet B (UVB).

Solar radiation is a key meteorological parameter for estimating the heating/cooling load of buildings [35] and for calculating the energy consumption of enclosures. In this case it is a fundamental parameter for assessing the degradation of the colour of the material. In the same way that the solar radiation received by a solar photovoltaic panel is affected by its orientation and tilt angle [36], both factors are corroborated in order to know the real degree of effect on the surface of the material. The measurements of the global and diffuse radiation fluxes on each façade have been measured with a CMP 3 pyranometer (Figure 1).

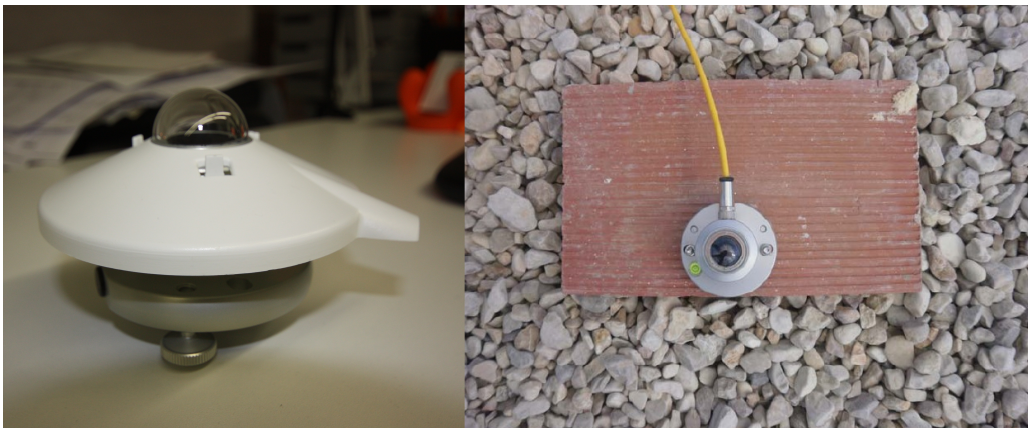

Figure 1. Left. Photo CMP 3 pyranometer. Right. CMP 3 Pyranometer installed on deck.

Through the statistical analysis of historical weather reports by time and model reconstructions from 1 January 1980 to 31 December 2016, different conditions are established according to the orientations of the façades. The average hourly wind vector of the wide area (speed and direction) is measured at 10 metres above the ground. The detailed study of wind direction allows to further specify the direction and speeds of the wind and thus to know the order in which it affects the 4 façades of the building.

For the investigation of the colourimetry of the material studied, a tele-spectroradiometer study was carried out, using a combination of 2 measurements: that of the ideal target and that of the sample. The ratio of the two measurements gives the intrinsic properties of the façade material in each of the building's orientations using the east side as a reference.

Once the measures had been taken on site, three different analyses were carried out:

- Spectral Radiance Analysis
- Spectral Reflectance Analysis
- Analysis of colourimetry and colour differences

4. Description of the Case Study

The building under study is located on the first line of the coast, in Playa de San Juan. It is part of the Urbanization La Rotonda complex and consists of 17 floors with 4 flats per floor. The tower was designed in 1965 by the architect J. Guardiola Gaya (Figure 2). It is the reference point at the beginning of San Juan beach, as well as being an architectural landmark in the architecture of the sun in the sixties. The formal structure of this tower has been influenced by a trip to Japan made by the architect a short time before. It is configured as a large prism-pagoda that acts as an urban landmark that marks the beginning of San Juan beach. Its sloping parapets in the shape of a ship's prow had already lost their original ceramic stoneware cladding [37], so in the 1990s the outer face of the parapets was restored with mortar and stone plaster.

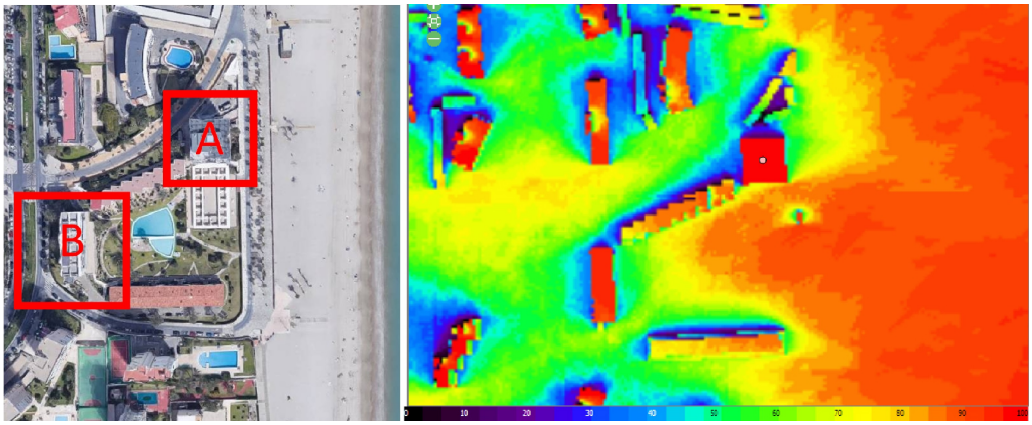

Figure 2. Left. Aerial photo of the La Rotonda complex. Block A–17 heights, Block B–6 heights Right: Sun footprint [38].

The triangular sloping parapets of the terraces were made of hollow brick, stabilised with a metal structure welded to the building's own metal structural system, and with internal metal reinforcements of platabandas and rounds. The interior finishing layer was formed by plastering and painting, while the exterior finish was plastered with projected stone, as can be seen in Figure 3. The problems of cracks in the mortar and stone enclosures with risk of detachment can be observed.

The balconies of each house are connected to each other by the metal structure of the building itself, which is attached to the railings.

The changes in temperature, the saline environment and the action of the wind caused an irreversible state. In 2010, due to the poor state of the parapets, they were replaced by others of similar geometry so as not to alter the image of the projected building, given its protection in the Catalogue of protected goods and spaces of Alicante City Council.

Figure 3. State of the building's façades and parapets in 2010, before its refurbishment.

The actions carried out were:

- Demolition of the original parapets.
- Replacement or reinforcement. In those elements whose material loss had been considerable, replacement was made with elements of similar mechanical and geometric characteristics. Those elements where replacement was not necessary were mechanically cleaned until the surface was completely sanitized.
- Anti-oxidant treatment. An anti-rust treatment was applied to the clean and smooth surface of the metal elements to support the new frame.
- Placement of auxiliary structure. The new parapet would be made up of a steel framing construction system, with lattice galvanised steel profiles similar to the original one, joined to the metal profiles of the perimeter structure of the building's floor, by means of metal elements as an extension of the profile wing. It was calculated for the own weight of the cladding and the wind actions for the exposed area according to the CTE- DB SE AE standard (Technical Building Code, Basic Document, Structural Safety, Actions in the building) (Figure 4).
- New coating. The exterior cladding was made of acrylic resin and natural mineral plates of variable height and similar geometry to the original parapets. White was chosen to minimise the degradation of the material [39]. The standard Corian® panels (3.66 × 0.93 m) were cut in the workshop and the 9 trapezoidal pieces that made up each parapet were assembled, joined and sanded on site with the appropriate safety measures for risks of pulmonary fibrosis associated with aluminium trihydrate [40]. The joints were reinforced at the back by 10 cm wide and 12 mm thick pieces. The result was a single piece more than 8 metres long which, in accordance with its coefficient of expansion, was screwed to the substructure by means of butt joints every 40 cm. The largest panel used up to that point. For its distribution, the tensile strength studies of the PMMA/ATH panels carried out by Nie et al. were taken into account [35]. These showed a 70% reduction in tensile strength when the sample was heated to 90 °C (Figure 5).
- Rigidisation of the parapets. To stiffen the parapets to horizontal movements, a pair of steel rounds, in the shape of a cross, was placed between the maximum length uprights.
- Placement of the acrylic and natural mineral plates. Once the sub-structure of the parapet was in place, the plates were placed on the inside and outside (Figure 6).

Figure 4. External coating. Exploded view of the Corian® sills and location of the profiles and anchors.

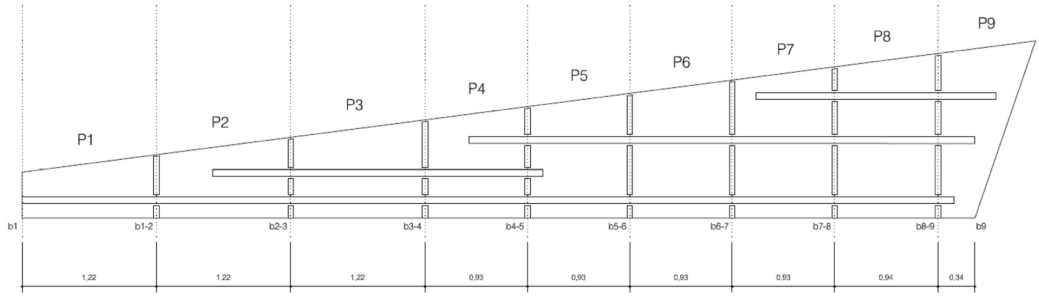

Figure 5. Top left image of the state of the supporting structure. In the rest of the images, substitution by galvanised structure, lifting of shaped piece on site and general view of the façade.

Figure 6. Images of interior and exterior finishing plate placement.

5. Data Collection

5.1. Wind

The percentage of hours in which the average wind direction comes from each of the four cardinal points in correspondence with the orientations of the façades, excluding the hours in which the average wind speed is less than 1.6 km/h, is plotted [41]. The light coloured areas at the boundaries are the percentage of hours of wind in the implied intermediate directions (north-east, south-east, south-west and north-west).Figure 7 shows the 12 months of the year and the summary table. Clearly the predominant wind is from the east.

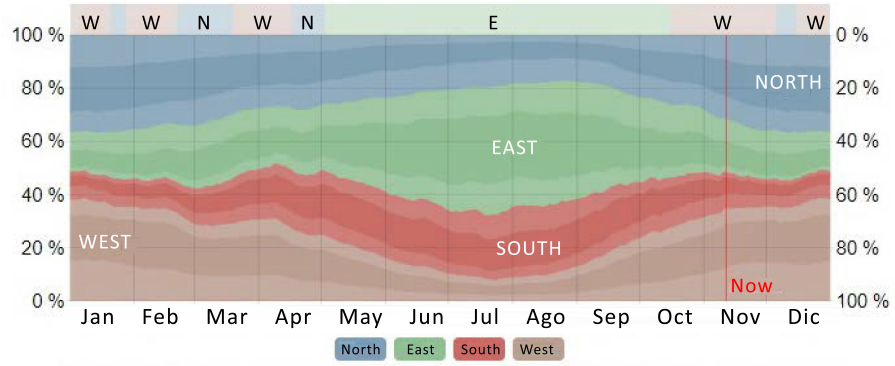

Figure 7. Predominance of dominant winds in building location.

The data provided by the previous study made it possibleto forecast a predominant direction of the East component wind, followed by West, North and South in the percentages shown in Table 1.

Table 1. Annual summary of winds predominance in building location [37].

	WEST	SOUTH	EAST	NORTH
Predominance of winds	61.79%	48.11%	75.87%	60.76%

Thanks to the wind rose, it is possibleunderstand more precisely the orientation of the winds on the building. The direction of the predominant winds at the location of the building results in a greater predominance of winds between 10 and 50 Km/h in the direction of the east face (Figure 8). This façade would be the most affected by wind and wear in the presence of aggressive atmospheric elements, above all due to the proximity of the sea (humid and saline air, etc.). The research carried out by Choi, E. [12,42] gave an idea of the importance of this circumstance. This reason leads to perform the test on the east façade of block B of the same plot to check if the damage caused by wind and particles is similar. The orientation is the same but at a greater distance from the sea front. This new measurement shows that the effect is similar, so that the predominance of easterly winds and the location of the beach in that area, means a greater sanding of the facade The particular circumstances of the location of the building on the San Juan beach favor that the side most exposed to the wind is also the most exposed to the sandblasting process due to the location of the beach. This new measurement allows to verify that the effect is similar. What most affects this side is the constant pressure of the wind, and therefore the sandblasting beyond the gusts that increase the speed punctually.

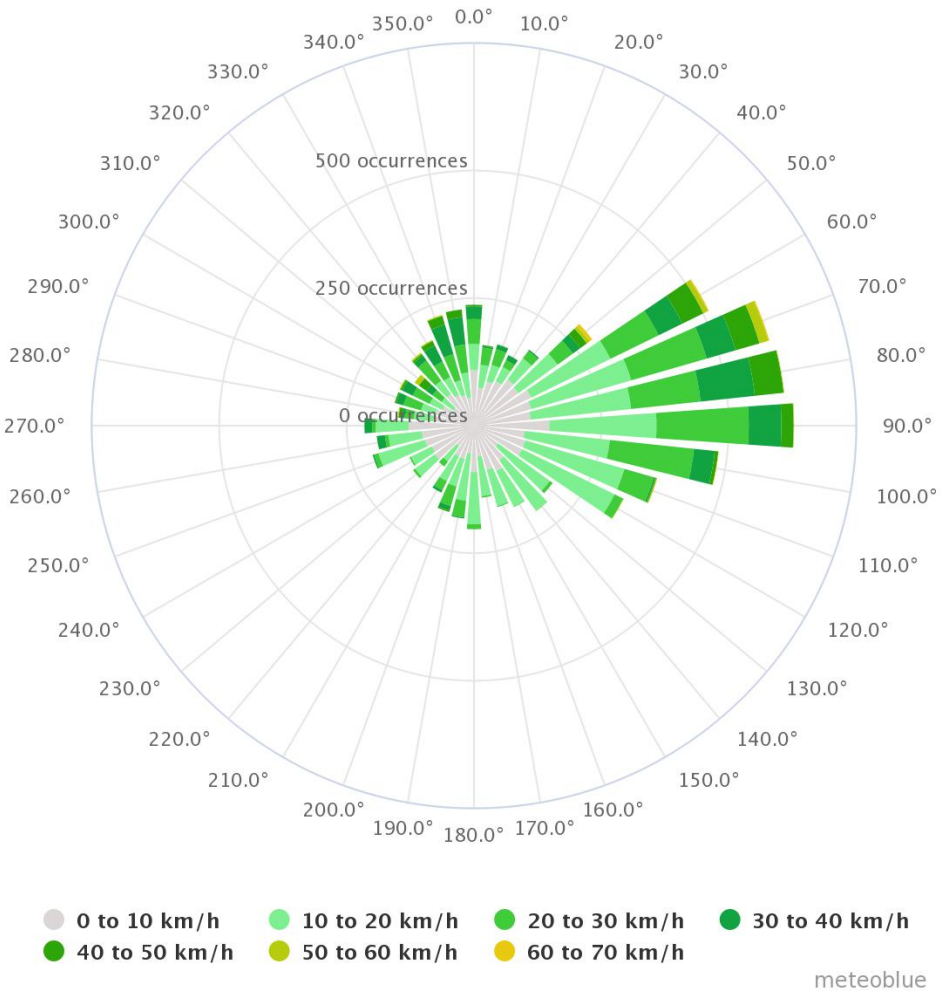

Figure 8. Wind Rose with dominant winds in building location. (Copyright Meteoblue.) [43].

5.2. Solar Radiation

Solar radiation is a fundamental aspect to take into account as a condition for improving the energy efficiency of our buildings. Numerous studies emphasise the importance of orientation according to the type of façade and the objectives to be achieved, in plant façades [39], solar façades [44].

The Climate Consultant software was used as a first approximation. The direct, diffuse and global average and total annual radiation of the 4 facades were analyzed. The data provided by Climate Consultant allow to sort the facades according to radiation. From the highest to the lowest received radiation the order is East, South, West and North (Figure 9).

The contrast of the initial data with the real measurements allows to refine the values and to detect errors in the use of models for diagnosis [45]. A significant change appears when measuring the direct, diffuse and global radiation of the 4 façades with their orientations from 2010 using a pyranometer model CMP 3. Figure 10 shows an annual cyclicity with similar values.

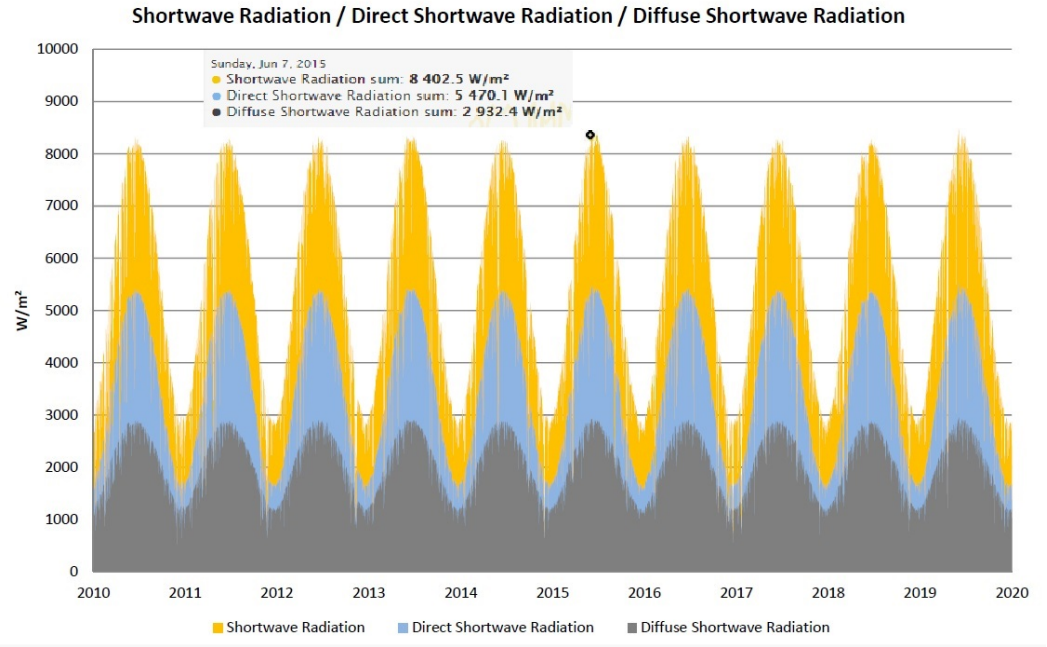

Figure 9. Direct and diffuse radiation from 2010 to 2020

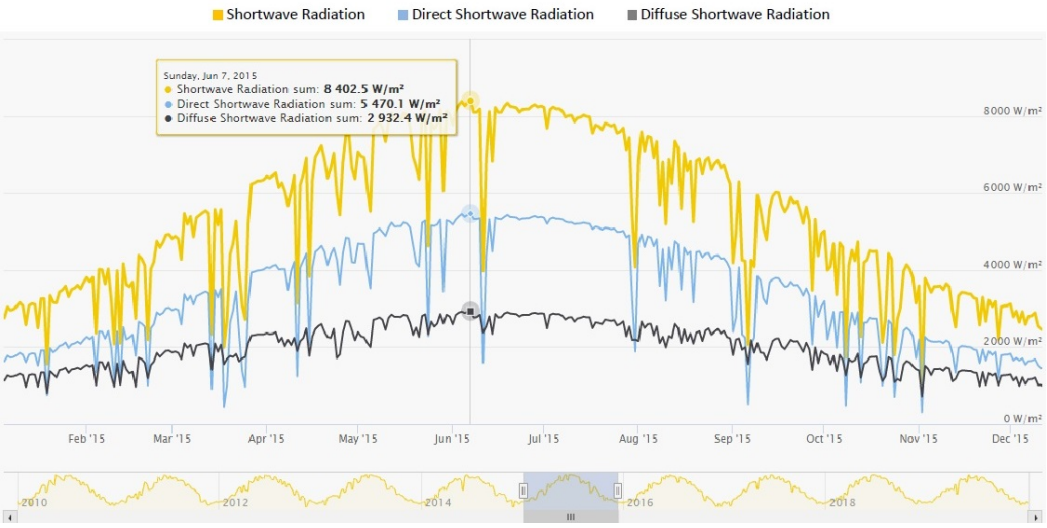

Figure 10. Shortwase, Direct and Diffuse radiation at 2015 with maximun value.

The higuest annual radiation received by the building in 2015 is shown in Figure 10. The highest radiation peak represented in yellow with 8402.5 W/m^2 is reached on June 7. In the historical series June is the month with the highest direct radiation. In contrast, the data show that the months with the lowest radiation are November and December with values between 23 W/m^2 and 102 W/m^2.

The temperature of the facades has never exceeded the manufacturer's limit of 100 °C. The material allows higher temperatures to be reached. Changes in bending properties occur between 100 °C and 160 °C [5]. Temperatures of 165 °C are usually used to be formed with forces of 100 KN [46]. The data it yields allows to sort according to radiation from highest to lowest in South/East/West and North.

The annual radiation received by the building is shown in Figure 11. The data it gives allows to order the radiation from highest to lowest in South/East/West and North Table 2.

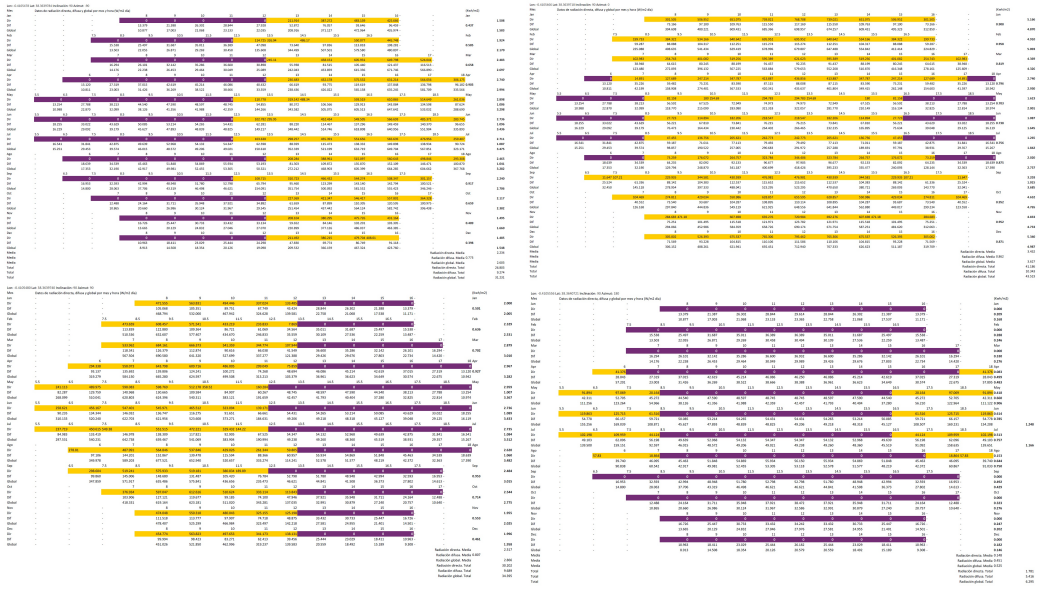

Figure 11. Annual radiation graphs of each façade measured with a pyranometer.

Table 2. Summary of average and total annual direct, diffuse and global radiation for each façade.

	NORTH	EAST	SOUTH	WEST
Direct radiation. Media	0.148	2.517	3.432	2.234
Diffuse radiation. Media	0.451	0.807	0.862	0.773
Global radiation. Media	0.525	2.866	3.627	2.603
Direct radiation. Total	1781	30.202	41.186	26.803
Diffuse radiation. Total	5416	9.689	10.343	9.274
Global radiation. Total	6295	34.395	43.523	31.231

5.3. Colourimetric Quantitative Analysis and Numerical Models

The measurements were taken with a tele-spectroradiometer on Thursday 23 January 2020, with completely clear skies, and between 11:45 and 12:45 in the morning Figure 12.

Figure 12. Measurement images of exterior finish plate.

6. Methodology

6.1. Test 1: Spectral Radiance

For the analysis of spectral radiances, one measurement per façade/orientation was made, and the following graph was obtained for the measurement of both the ideal target and the sample (in the same position and orientation of the instrument), as shown in Figure 13.

After measuring each façade of its four orientations, it is obtained that the initial spectral radiances of both the target and the sample (in the same position and orientation of the instrument) are.

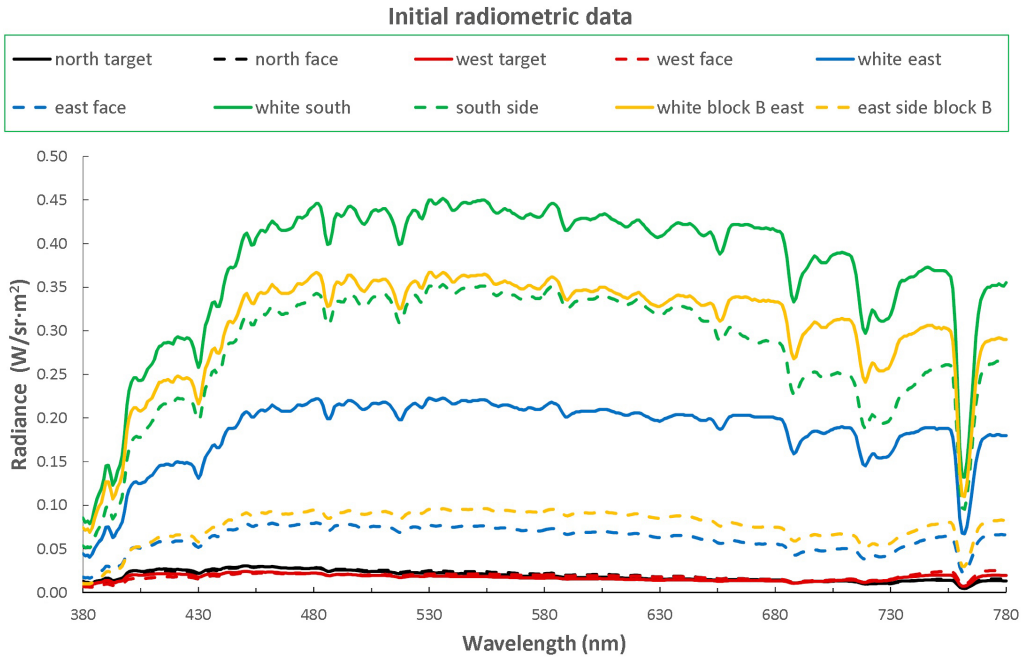

Figure 13. Daylight spectrum, with its gentle ripples of gas absorption in the atmosphere.

Below is a detailed analysis of each of the 4 sides of the building:

- North Face: according to the graph in Figure 14, the material's fluorescent behaviour can be seen. This is mainly due to the fact that in some spectral bands, specifically from 480 to 680 nm, the radiance emitted by the material is higher than that of the ideal target in the same position and orientation. It can be seen then that the differences between both spectra are smaller so that the reflectance factor of the material on the east side will be above 1 in some spectral bands.
- West side: according to the graph shown in Figure 15, the fluorescent behaviour of the material on this side can be seen. As in the east side in some spectral bands, from 480 to 680 nm, the radiance emitted by the material is higher than that of the ideal target in the same position and orientation. The differences between the two spectra are therefore smaller, which will give a factor of reflectance of the material on the north face above 1 in some spectral bands. In other words, both the north and west faces appear optically and colourimetrically very similar.

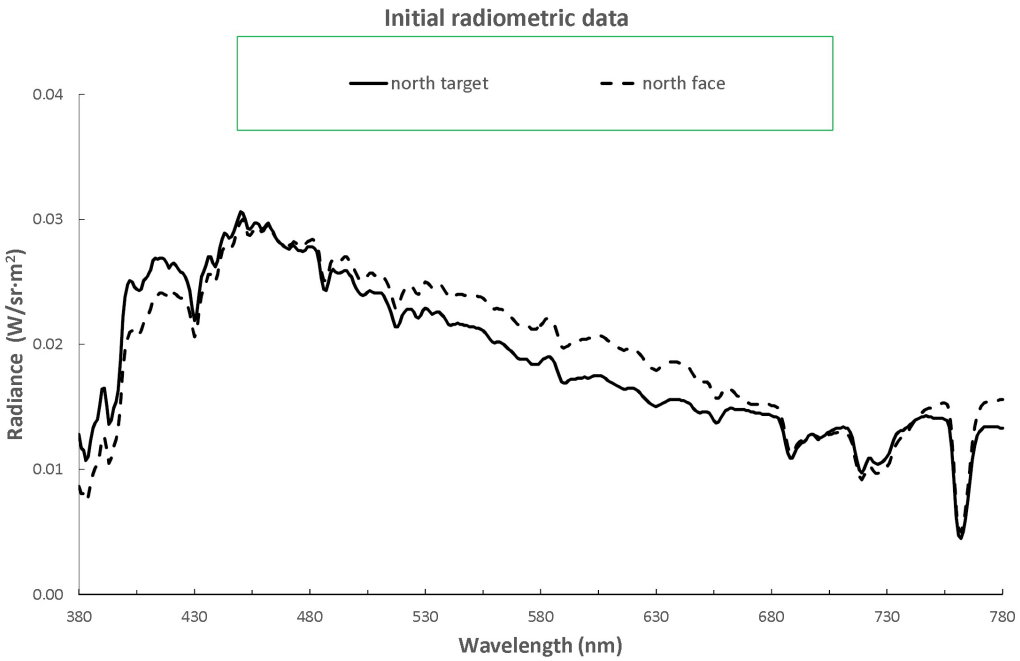

Figure 14. North face radiometric data.

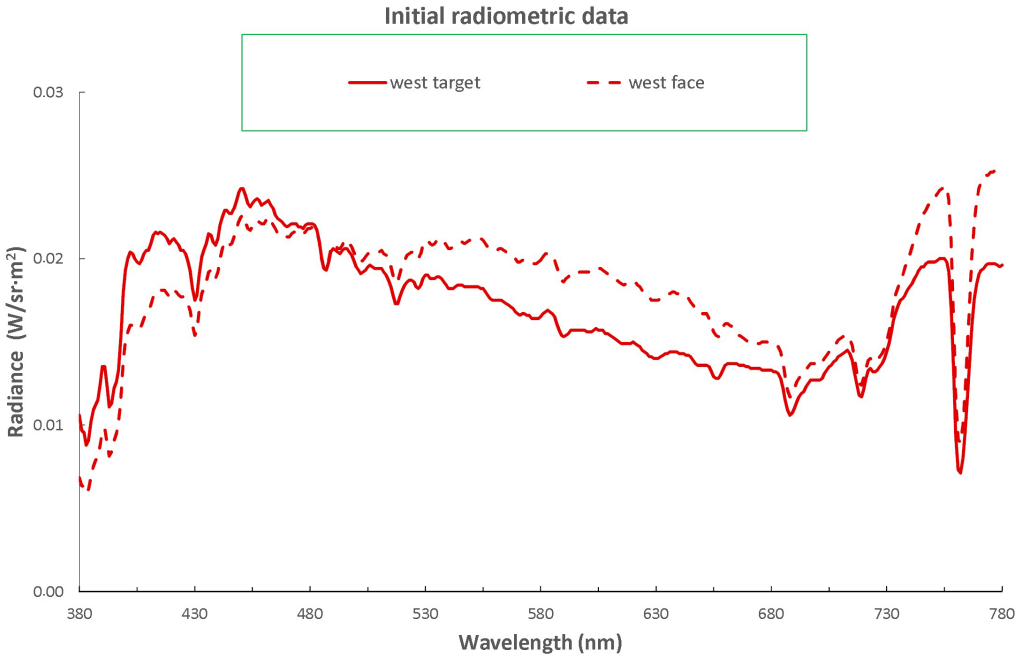

Figure 15. West side radiometric data.

- East side: according to the graph in Figure 16, the spectral and optical behaviour is different from the two previous sides analysed. In this case the material (façade) always radiates less than the white in the same position and orientation. Therefore, in principle, there would be no fluorescent behaviour. On the other hand, the differences in height of the white vs. façade spectra are notable, implying that the material of the east façade will no longer be optically and colourimetrically the same or similar to the north and west façcades, which implies a darkening of the material, which will be analysed later.

- In addition to the east side of the 17-storey tower, measurements were taken of the façade of the 6-storey block B located in the same area with the same orientation, situated slightly to the left, set back on a slight slope, and also with views of the sea.

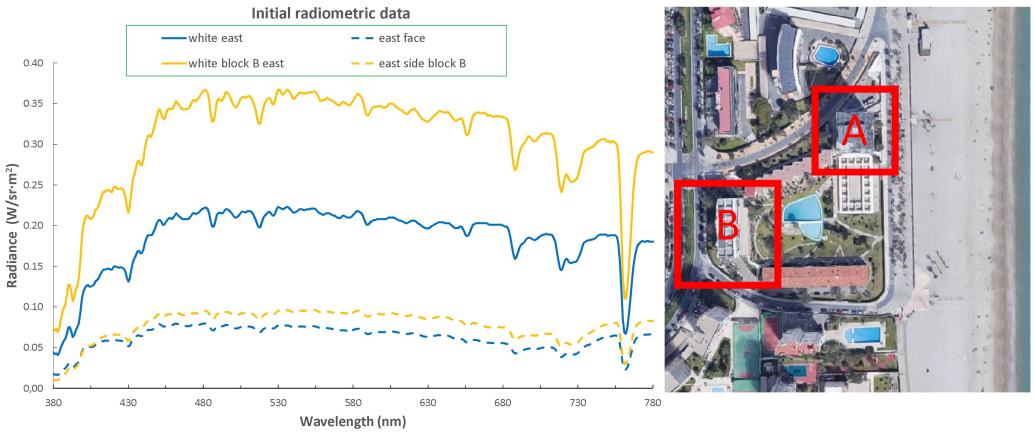

Figure 16. Location of blocks A and B. Radiometric data for this block B.

- South Face: this façade has a spectral and optical behaviour similar to that of the east façade, but not as pronounced in the darkening of the material Figure 17.

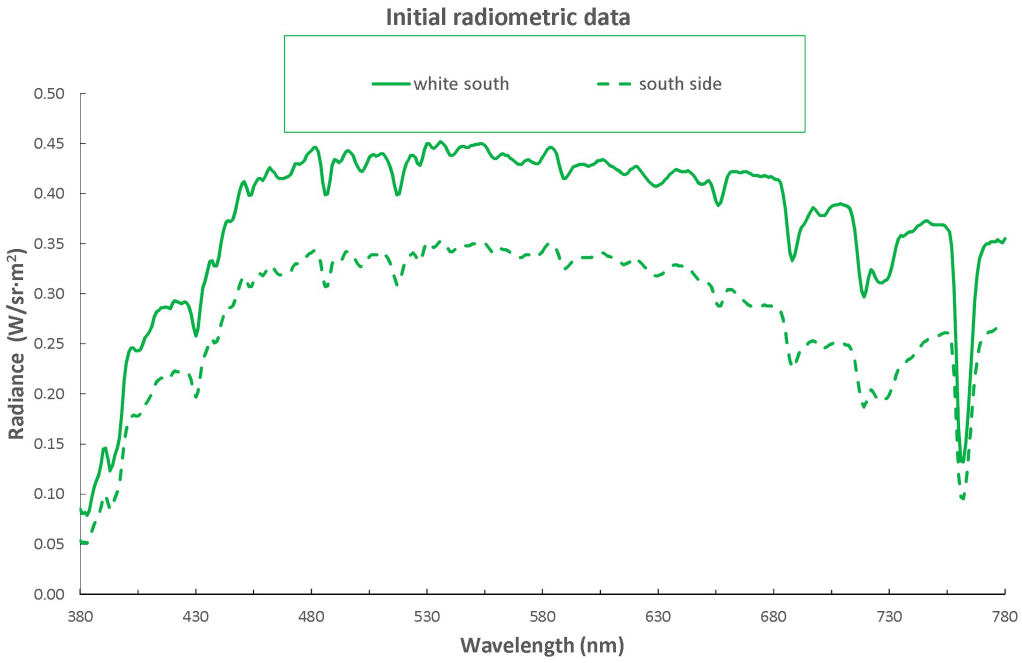

Figure 17. South-facing radiometric data.

6.2. Test 2: Spectral Reflectances

With regard to the analysis of the spectral reflectances (Figure 18), taking into account the ratio between the radiances of the sample versus the white colour, the following results were obtained:

- The north and west faces are very similar in spectral reflectance;
- The south side is darker than the west and north sides;
- The east side (in the two blocks analysed) is darker than the south side and therefore much darker than the west and north sides.

- Furthermore, as there are spectral reflection curves that are not strictly parallel to each other, there are also differences in tone and colour, but not as great as in clarity.

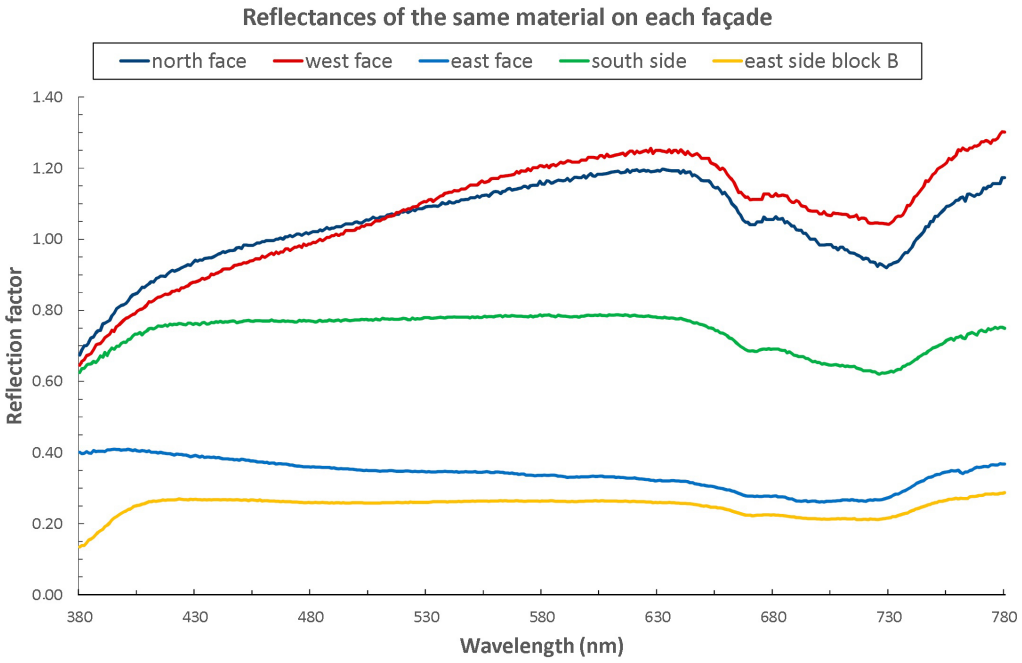

Figure 18. Analysis of CIE colourimetry.

6.3. Test 3: Colourimetry and Colour Differences

For the study of colourimetry and colour differences, CIE-L*a*b*Cab*hab colourimetry has been applied, always using as a standard target the one corresponding to the Sun (ideal target) in each orientation. In addition, the east side has been used as a reference for the rest of the building's faces. The visual results simulated in RGB with a calibrated monitor (sRGB) are as follows (Figure 19).

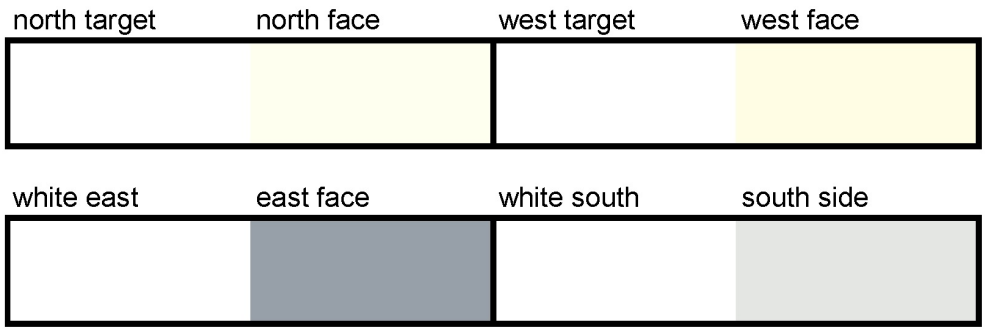

Figure 19. Visual results simulated in RGB with a calibrated monitor (sRGB) are as follows.

The differences in colour DEab, and DECIE2000, with respect to the north face are shown in Table 3.

Table 3. Colour differences DEab, and DECIE2000 with respect to the north face.

	North	West	This	South	East 2
DL	0.00	1.07	−39.33	−13.58	−46.17
Da	0.00	0.15	−0.17	0.18	0.62
Db	0.00	4.76	−13.49	−8.03	−9.40
DCab	0.00	4.74	−4.41	−7.96	−8.57
Dhab	0.00	−1.94	166.44	19.90	178.79
DHab	0.00	0.38	12.75	1.05	3.90
DEab	0.00	4.88	41.58	15.78	47.12
DECH	0.00	4.88	41.58	15.78	47.12
DE00	0.00	3.22	28.60	10.31	32.52

The data from the three analyses performed are shown in Table 3, which allows the following results to be obtained:

- The western side shows a very slight deviation in colour, more yellowish and slightly stronger, and almost as clear.
- The eastern face presents a very evident difference in clarity: it is notoriously very dark, hiding quite a few other more subtle differences in tone (+bluish) and colour (+weak). This is obtained equally, with the same order of magnitude, on the east side of block B. Let remember that wind analysis already showed a greater inclemency of the wind in this direction.

7. Discussion of Results

Simulation tools make simplifications by offering statistical data that do not conform to reality. Climate Consultant provided data that allowed the façades to be ordered according to radiation: from the highest to the lowest received radiation the order is East/South/West and North. However, research on the building allows to refine this data and check that the south side has the greatest number of hours of direct, diffuse and global radiation, followed by the east, west and north.

The monitoring of the wind direction on the four façades showed the East and South façades to be the most affected. The test with the tele-spectroradiometer shows that the darkening of the material is greater on the east side (in the two blocks analysed) than on the south side and much greater than on the west and north sides. They also present differences in tone and colour but to a lesser degree.

8. Conclusions

Analysis of data from radiation and wind studies after assessment of the degree of effect on the surface colour of Corian® after 10 years of exposure leads to the following conclusions.

The actions of the wind and the sun generate the greatest wear on the surface of Corian® material. The hours of solar radiation depending on the orientation of the façade, both daily and seasonally, and the particles in suspension in a saline environment, mainly sand, cause the differences according to orientation.

The material has suffered a degradation of the colour of its surface that is greater than the classification by Dupont which valued less than or equal to $5\Delta E^*_{ab}$ units of 5 to 15 years.

It is important to conclude that Corian is a very suitable material for use in façades with large format panelling because of its durability and stability. There is a small vulnerability in the material due to its exposure to atmospheric agents, saline environment and solar radiation, which alters the colour of its surface causing it to age over time.

The work presented here was developed in collaboration amongst all authors.

Author Contributions: Conceptualisation, Solar Radiation: C.R.-M.; data conservation, M.I.P.-M.; formal analysis Wind study: V.E.-I.; Funding acquisition, Research, A.G.-G. and M.I.P.-M.; Methodology, Á.B.G.-A. and V.E.-I.; Project administration, A.G.-G.; Resources, A.G.-G.; Supervision, A.G.-G.

and C.R.-M.; Validation, Á.B.G.-A.; Visualisation, C.R.-M.; Writing, original draft, Á.B.G.-A.; Writing, revision and editing, Á.B.G.-A.; V.E.-I. and A.G.-G. Colour analysis and sample taking; V.E.-I., Wind study; C.R.-M., Solar radiation study; C.R.-M., Solar radiation study and bibliographic sources; M.I.P.-M. historical compilation and monitoring in progress. All authors have read and agreed to the published version of the manuscript.

Funding: This research received no external funding.

Acknowledgments: Our thanks to Miguel Salvador Landmann and Antonio Salmerón Martínez for access to technical project documentation and photographs. Also to Francisco Miguel Martínez Verdú, Vision and Colour Group of the University of Alicante.

Conflicts of Interest: The authors declare no conflict of interest.

References

1. Ansah, M.K.; Chen, X.; Yang, H.; Lu, L.; Lam, P.T.I. An integrated life cycle assessment of different façade systems for a typical residential building in Ghana. *Sustain. Cities Soc.* **2020**, *53*, 101974. [CrossRef]
2. Kovacic, I.; Waltenbereger, L.; Gourlis, G. Tool for life cycle analysis of facade-systems for industrial buildings. *J. Clean. Prod.* **2016**, *130*, 260–272. [CrossRef]
3. Bruce-Hyrkäs, T.; Pasanen, P.; Castro, R. Overview of Whole Building Life-Cycle Assessment for Green Building Certification and Ecodesign through Industry Surveys and Interviews. *Procedia CIRP* **2018**. [CrossRef]
4. Balali, A.; Valipour, A. Identification and selection of building façade's smart materials according to sustainable development goals. *Sustain. Mater. Technol.* **2020**, *26*, e00213.
5. Tawalbeh, M.; Al-Othman, A.; Kafiah, F.; Abdelsalam, E.; Almomani, F.; Alkasrawi, M. Environmental impacts of solar photovoltaic systems: A critical review of recent progress and future outlook. *Sci. Total Environ.* **2020**, 143528. [CrossRef] [PubMed]
6. Talaei, M.; Mahdavinejad, M.; Azari, R. Thermal and energy performance of algae bioreactive façades: A review. *J. Build. Eng.* **2020**, *28*, 101011. [CrossRef]
7. Li, C. Experimental thermal performance of wallboard with hybrid microencapsulated phase change materials for building application. *J. Build. Eng.* **2020**, *28*, 101051. [CrossRef]
8. Ren, M.; Liu, Y.; Gao, X. Incorporation of phase change material and carbon nanofibers into lightweight aggregate concrete for thermal energy regulation in buildings. *Energy* **2020**, *197*. [CrossRef]
9. Mukhamet, T.; Kobeyev, S.; Nadeem, A.; Memon, S.A. Ranking PCMs for building façade applications using Multi-Criteria Decision-Making tools combined with energy simulations. *Energy* **2020**, *215*, 119102. [CrossRef]
10. Perez, R.; Ineichen, P.; Seals, R.; Michalsky, J.; Stewart, R. Modeling daylight availability and irradiance components from direct and global irradiance. *Sol. Energy* **1990**, *44*, 271–289. [CrossRef]
11. Gaspar, P.L.; de Brito, J. Quantifying environmental effects on cement-rendered facades: A comparison between different degradation indicators. *Build. Environ.* **2008**, *43*, 1818–1828. [CrossRef]
12. Choi, E.C.C. Simulation of wind-driven-rain around a building. *J. Wind Eng. Ind. Aerodyn.* **1993**, *46–47*, 721–729. [CrossRef]
13. Byrdy, A.; Kołaczkowski, M. Environmental Impacts on the Strength Parameters of Mineral-Acrylic (PMMA/ATH) Facade Panels. *Int. J. Polym. Sci.* **2015**, *2015*. [CrossRef]
14. Pereira, C.; de Brito, J.; Silvestre, J.D. Contribution of humidity to the degradation of façade claddings in current buildings. *Eng. Fail. Anal.* **2018**, *90*, 103–115. [CrossRef]
15. Chew, M.Y.L.; Tan, P.P. Facade staining arising from design features. *Constr. Build. Mater.* **2003**, *17*, 181–187. [CrossRef]
16. Mohaney, P.; Soni, E.G. Aluminium Composite Panel as a Facade Material. *Int. J. Eng. Trends Technol.* **2018**, *55*. [CrossRef]
17. Harhash, M.; Gilbert, R.R.; Hartmann, S.; Palkowski, H. Experimental characterization, analytical and numerical investigations of metal/polymer/metal sandwich composites—Part 1: Deep drawing. *Compos. Struct.* **2018**, *202*, 1308–1321. [CrossRef]
18. N./English and Corian®. Corian® Solid Surface Technical Bulletin Corian® Solid Surface Material Composition. 2018. Available online: https://www.corian.com/IMG/pdf/k-30025-corian-solid-surface-material-composition-bulletin_sec.pdf (accessed on 29 January 2021).
19. Qi, C.; Echt, A.; Murata, T.K. Characterizing dust from cutting corian®, a solid-surface composite material, in a laboratory testing system. *Ann. Occup. Hyg.* **2016**, *60*, 638–642. [CrossRef]
20. Kang, S.; Liang, H.; Qian, Y.; Qi, C. The Composition of Emissions from Sawing Corian®, a Solid Surface Composite Material. *Ann. Work Expo. Heal.* **2019**, *63*, 480–483. [CrossRef]
21. Wronka, A.; Kowaluk, G. Selected bending properties of mineral-acrylic solid surface material for furniture construction purposes. *Ann. WULS, For. Wood Technol.* **2020**, *110*, 54–60. [CrossRef]
22. Jackson, A.P.; Vincent, J.F.V.; Turner, R.M. Comparison of nacre with other ceramic composites. *J. Mater. Sci.* **1990**, *25*, 3173–3178. [CrossRef]
23. Andriievska, L.; Marchuk, N. Investigation of the acrylic artificial stone properties. *Technol. Innov. Princ. Tech. Solut.* **2017**, *0*, 21–23. [CrossRef]

24. Basaran, C.; Nie, S.; Hutchins, C.S. Time Dependent Behavior of a Particle Filled Composite PMMA/ATH at Elevated Temperatures. *J. Compos. Mater.* **2008**, *42*, 2003–2025. [CrossRef]
25. Mackey, L.T.; Wright, C.O. Periodic heat flow-composite walls or roofs. *Trans. Am. Soc. Heat. Vent. Eng.* **1946**, *52*, 283–304.
26. Basaran, C.; Nie, S. A thermodynamics based damage mechanics model for particulate composites. *Int. J. Solids Struct.* **2007**, *44*, 1099–1114. [CrossRef]
27. Pickering, E.G.; O'Masta, M.R.; Wadley, H.N.G.; Deshpande, V.S. Effect of confinement on the static and dynamic indentation response of model ceramic and cermet materials. *Int. J. Impact Eng.* **2017**, *110*, 123–137. [CrossRef]
28. DuPont ^{TM}Corian® Exterior Cladding Dupont TM Corian® Exterior Cladding Innovation in Architecture. Available online: https://www.corian.tw/IMG/pdf/dupont-corian-cladding.pdf (accessed on 29 January 2021).
29. ASTM D2244-07 Calculation of Color Tolerances and Color Differences From Measured Color Coordinates | Hue | Color. Available online: https://es.scribd.com/document/401129863/ASTM-D2244-07-Calculation-of-Color-Tolerances-and-Color-Differences-From-Measured-Color-Coordinates (accessed on 10 November 2020)
30. Dozić, A.; Kleverlaan, C.J.; Aartman, I.H.A.; Feilzer, A.J. Relation in color among maxillary incisors and canines. *Dent. Mater.* **2005**, *21*, 187–191. [CrossRef] [PubMed]
31. Venkatasubramanian, V.; Rengaswamy, R.; Yin, K.; Kavuri, S.N. A Review of Process Fault Detection and Diagnosis Part I: Quantitative Model-Based Methods. Available online: https://www.ece.lsu.edu/mcu/lawss/add_materials/FaultDetectionPart1.pdf (accessed on 27 November 2020)
32. N./English, Dupont^{TM} Corian® Solid Surface Technical Bulletin Colorfastness and Exterior Use of Dupont ^{TM} Corian® Solid Surface. 2016. Available online: https://www.corian.com/IMG/pdf/k-27409_corian_solid_surface_colorfastness_and_exterior_use.pdf (accessed on 14 February 2020).
33. ASTM G155–00 Standard Practice for Operating Xenon Arc Light Apparatus for Exposure of Non-Metallic Materials. Available online: https://www.astm.org/DATABASE.CART/HISTORICAL/G155-00.htm (accessed on 14 February 2020).
34. Aruniit, A.; Kers, J.; Tall, K. Influence of filler proportion on mechanical and physical properties of particulate composite. *Agron. Res.* **2011**, *9*, 23–29.
35. Narla, S.; Kohli, I.; Hamzavi, I.H.; Lim, H.W. Visible light in photodermatology. *Photochem. Photobiol. Sci.* **2020**, *19*, 99–104. [CrossRef]
36. An, J.; Yan, D.; Guo, S.; Gao, Y.; Peng, J.; Hong, T. An improved method for direct incident solar radiation calculation from hourly solar insolation data in building energy simulation. *Energy Build.* **2020**, *27*, 110425. [CrossRef]
37. Demain, C.; Journée, M.; Bertrand, C. Evaluation of different models to estimate the global solar radiation on inclined surfaces. *Renew. Energy* **2013**. [CrossRef]
38. Gaya, J.G.; Meyer, J.O. 01-044. La Rotonda. via Arquitectura. 01. Available online: http://www.via-arquitectura.net/01/01-044.htm (accessed on 14 February 2020).
39. Huellasolar Visor OpenPlatform Huellasolar. Web Application. Sun and Radiation Maps of Cities. Available online: http://www.huellasolar.com/?page_id=4065&lang=es#mapview (accessed on 14 February 2020).
40. Ramos, N.M.M.; Souza, A.R.; Maia, J.; Almeida, R.M.S.F. Colour Degradation of Façade Coatings-the Effect of Nanopigments Incorporation. In Proceedings of the 12th Nordic Symposium on Building Physics (Nsb) in: 12th Nordic Symposium on Building Physics (Nsb 2020), Tallinn, Estonia, 7–9 September 2020; Available online: https://ui.adsabs.harvard.edu/abs/2020E3SWC.172240004R/abstract (accessed on 27 November 2020). [CrossRef]
41. Raghu, G.; Collins, B.F.; Xia, D.; Schmidt, R.; Abraham, J.L. Pulmonary fibrosis associated with aluminum trihydrate (Corian) dust. *N. Engl. J. Med.* **2014**, *370*, 2154–2157. [PubMed]
42. Certification "Avis Technique" ATEC 2/11-1472, Including Tests ISO 4892-2 (Accelerated Ageing), EN 14509 (Humidity Test), ISO 10545-12 (Resistance to Freeze-Thaw Cycles). Available online: https://www.corian.es/IMG/pdf/emea_corian_ec__french_certification.pdf (accessed on 27 November 2020).
43. Average Time in December in Alicante, Spain—Weather Spark. Available online: https://weatherspark.com/y/42586/Average-Weather-in-Alicante-Spain-Year-Round (accessed on 27 November 2020).
44. Rosa de los Vientos Alicante—Meteoblue. Available online: https://www.meteoblue.com/es/tiempo/archive/windrose/alicante_espa%C3%B1a_2521978 (accessed on 20 October 2020).
45. Holmes, J.D.; Baker, C.J.; English, E.C.; Choi, E.C.C. Wind structure and codification. *Wind. Struct.* **2005**, *8*, 235–250. [CrossRef]
46. Peng, H.; Li, M.; Li, Z.; Li, X. Surface quality and shape accuracy of multi-point warm press forming Corian sheets. *Int. J. Adv. Manuf. Technol.* **2019**, *104*, 4727–4733. [CrossRef]